Journal of Power Sources 191 (2009) 119–126

Contents lists available at ScienceDirect

Journal of Power Sources

journal homepage: www.elsevier.com/locate/jpowsour

Thermal behavior of VRLA battery during closed oxygen cycle operation

D. Valkovska*, M. Dimitrov, T. Todorov, D. Pavlov

Institute of Electrochemistry and Energy Systems, G. Bonchev Street, Block 10, BAS, 1113 Sofia, Bulgaria

ARTICLE INFO

Article history:
Received 9 September 2008
Received in revised form
29 September 2008
Accepted 1 October 2008
Available online 17 October 2008

Keywords:
Valve-regulated lead-acid battery
Thermal behavior
Overcharge
Oxygen evolution reaction

ABSTRACT

This paper presents the results of the investigations of the thermal behavior of a model valve-regulated lead-acid cell at overcharge and saturation level around 90%. The heat capacity and the heat transfer coefficient are experimentally obtained. The quasi-steady state characteristics of the cell at constant charging current are measured. The experimental data show that, when operating in recombination regime, the stationary cell temperature is a linear function of the charging current. When the cell is gassing, part of the heat is dissipated with the released gases, as a result of which the cell temperature is lower than predicted from the linear temperature/current dependence. Introduced dimensionless slope of the temperature/current dependence is a characteristic of the VRLA battery, which could be used for fast and easy estimation of the temperature increase of the battery. The kinetic parameters of the oxygen evolution reaction (OER) proceeding at the positive plates of VRLA cells are experimentally determined. The current/overpotential dependence of the OER obeys the Tafel relation. The temperature/current dependence and the kinetics of the OER are used to estimate the critical charging voltage for safe operation of the battery.

1. Introduction

The thermal behavior of lead-acid batteries, and especially of their recombinant versions, receives considerable attention in the context of its contribution to the heat generation in power systems, efficiency of operation, reduction in service life and susceptibility to thermal runaway. The thermodynamics of the primary reactions in a lead-acid cell is described in [1]. The thermal "vicious cycle" of vented batteries with low heat transfer, caused by secondary reactions of water electrolysis during overcharge, is analyzed in [2]. Thermal runaway is a result of the positive feedback between the heat generation due to Joule losses and the rate of Arrhenius gas evolving reactions during water electrolysis.

The heat generation in recombinant VRLAB on overcharge is discussed in [3], where in addition to electrolysis, the internal oxygen cycle in which the full power of the charging unit is used only for heating, is considered. The VRLA battery on overcharge can be generally treated as parallel-connected electrolyser and oxygen generator/recombinator. The thermal stability of the VRLA battery is determined by its reduced thermal mass and thermal conductivity of the interior as part of the electrolyte is replaced by gas, both decreasing with drying [4,5]. Stability analysis of VRLA batteries subjected to abusive tests in high temperature-high overcharge voltage environment is performed and the obtained results are discussed in refs. [5–8]. The influence of a preceding discharge/charge cycle on the thermal instability is demonstrated in [4,9,10,11]. Investigations of the thermal phenomena have been developed in several areas as thermal mapping [7] to visualize the temperature distribution inside the cell; thermal video imaging and calorimetric measurements [12–14] to study the thermal problems arising in EV and HEV batteries; several electrochemical studies have been performed to elucidate the influence of separator structure [15], saturation level [16,17] and electrolyte distribution in separator [11]; the important role of the mechanisms of oxygen evolution and recombination on thermal runaway is discussed in [18–22]; thermal management systems have been proposed [4,5,23,24].

The aim of the present work was to evaluate the quasi-steady state characteristics of a VRLA battery during overcharge. To achieve this goal we measured:

(a) the heat capacity, C_p, and overall heat transfer coefficient, h, of the battery;
(b) the quasi-stationary characteristics of the system and obtained stationary T vs. I curves by performing a series of stepwise constant current polarization experiments;
(c) the kinetics of the oxygen evolution reaction proceeding at the positive plates of VRLA batteries.

Based on the obtained results, we discuss the conditions for possible thermal failure of the battery.

* Corresponding author. Tel.: +359 2 9792720; fax: +359 2 8731552.
E-mail address: dvalkovska@bas.bg (D. Valkovska).

0378-7753/$ – see front matter © 2008 Elsevier B.V. All rights reserved.
doi:10.1016/j.jpowsour.2008.10.014

2. Charge and discharge reactions and thermal behavior of VRLA batteries

A VRLA battery consists of $Pb/PbSO_4$ negative electrodes, $PbO_2/PbSO_4$ positive electrodes, absorptive glass mat (AGM) separator and H_2SO_4 electrolyte. The electrochemical reactions that take place at each electrode during cell operation can be summarized as follows (left to right are the charge reactions, and in the reverse direction are the discharge reactions.):

Positive electrode ($PbO_2/PbSO_4$):

$$PbSO_{4(s)} + 2H_2O \leftrightarrow PbO_{2(s)} + HSO_4^- + 3H^+ + 2e^- \quad (1)$$

with oxygen evolution

$$2H_2O \rightarrow O_2 + 4H^+ + 4e^- \quad (2)$$

hydrogen recombination

$$H_2 \rightarrow 2H^+ + 2e^- \quad (3)$$

and grid corrosion

$$Pb + 2H_2O \rightarrow PbO_2 + 4H^+ + 4e^- \quad (4)$$

Negative electrode ($Pb/PbSO_4$):

$$PbSO_{4(s)} + H^+ + 2e^- \leftrightarrow Pb_{(s)} + HSO_4^- \quad (5)$$

with oxygen recombination

$$O_2 + 4H^+ + 4e^- \rightarrow 2H_2O \quad (6)$$

and hydrogen evolution

$$2H^+ + 2e^- \rightarrow H_2. \quad (7)$$

Reactions (2), (3), (6) and (7) constitute the internal oxygen and hydrogen cycles in the cell. In the presence of these side reactions, the VRLA cell is a three-phase system consisting of the solid matrix, liquid electrolyte and gas phase. At the end of charge and during overcharge, oxygen is generated at the PbO_2/electrolyte interface and may evolve in the gas space when its solubility limit in the electrolyte is exceeded. The oxygen can then be transported, via the liquid and gas phases, from the positive to the negative electrode, where the oxygen gas may dissolve back in the electrolyte and be reduced at the Pb/electrolyte interface. This process forms the internal oxygen cycle in VRLA batteries.

Even though the oxygen evolution reaction on the positive plate is, in general, a multi-step process, it can be expressed by the overall reaction (2). The oxygen reduction reaction on the negative plate, however, is much more complex. Although in most cases it is faster and predominates over the hydrogen evolution reaction, reactions (6) and (7) are always in competition. A detailed description of the different possible mechanisms of oxygen reduction at the negative plate is given in [18–22]. Here, we will consider only the simplest mechanism described by Eqs. (6) and (7).

Hydrogen is generated according to reaction (7) at the negative electrode, when the electrode potential goes too low (polarization becomes high). Hydrogen recombination, as described by Eq. (3), is negligible because of its poor kinetics [25,26]. Accumulation of oxygen and hydrogen in the gas phase contributes to pressure build up, thereby causing venting.

Grid corrosion depends on electrode potential in a complex way. If the potential of the positive electrode rises, starting from its open circuit value, grid corrosion decreases in the beginning, reaches a minimum, and increases again [27–29]. Compared to the OER, the kinetics of the grid corrosion reaction is much slower.

Heat source terms: As we are interested only in the overcharge process, the main charge/discharge reactions (1) and (5) do not take place, and hence only the oxygen and hydrogen cycles are operative.

Table 1
Thermodynamic properties of VRLA battery.

Symbol	Value	Unit	Description
ΔS_2	+326.412	$J K^{-1} mol^{-1}$	Entropy change of reaction (2)
ΔS_6	−326.412	$J K^{-1} mol^{-1}$	Entropy change of reaction (6)
ΔS_7	0	$J K^{-1} mol^{-1}$	Entropy change of reaction (7)
$\varphi^0_{O_2}$ (25 °C)	1.229	V	Standard potential of O_2/H_2O at 25 °C towards SHE
φ^0_{Ag/Ag_2SO_4} (25 °C)	0.654	V	Standard potential of Ag/Ag_2SO_4 at 25 °C towards SHE
$\left(d\varphi/dT\right)_{O_2/H_2O}$	−0.846	$mV K^{-1}$	Isothermal temperature coefficient of standard potential of O_2/H_2O
$\left(d\varphi/dT\right)_{Ag/Ag_2SO_4}$	−1.182	$mV K^{-1}$	Isothermal temperature coefficient of standard potential of Ag/Ag_2SO_4

During overcharge of the VRLA cell, the total heat generation rate, Q_{cell}, is a sum of the rates of the endothermic and exothermic heat generated due to entropy changes of the electrochemical reactions, Q_S, the ohmic heat generated due to the resistance of the electrolyte and the solid matrix, Q_{Ohm}, and the exothermic heat generated by overpotentials resulting from the shift from the electrochemical equilibriums of the reactions, Q_η. The enthalpy of water evaporation is neglected. The sum $Q_\eta + Q_{Ohm}$ represents the Joule (irreversible) heat.

$$Q_{cell} = Q_S + Q_{Ohm} + Q_\eta. \quad (8)$$

As we consider only the simplest electrochemical mechanisms of O_2 evolution and reduction, the above terms are described as follows:

(a) Entropy term:

$$Q_S = -\sum_i T \frac{\Delta S_i}{n_i F} \left|I_i\right| \quad (9)$$

which is summed over the electrochemical reactions proceeding in the cell. T is the cell temperature, ΔS_i is the entropy change of reaction i, F is the Faraday constant, n_i is the number of electrons exchanged by the ith electrochemical reaction, and I_i stands for the reaction currents. In our system, only three electrochemical reactions proceed during overcharge: reaction (2) at the positive electrode and reactions (6) and (7) at the negative one. Hence,

$$I_2 = I_{O_2} = I \quad (10a)$$

$$I_6 = I_{O_2,rec} = -\gamma I \quad (10b)$$

$$I_7 = I_{H_2} = -(1-\gamma) I \quad (10c)$$

γ is a measure for the relative contribution of the oxygen and hydrogen reactions to the cell current at the negative plate. It gives the efficiency of the oxygen cycle. When the oxygen recombination reaction is predominant, γ tends to 1, while when hydrogen evolution is operative, γ decreases. The latter happens when the negative plate becomes highly polarized, in which case usually the cell is gassing. The values of ΔS_i are listed in Table 1 [30]. For calculation of ΔS_i the value of the entropy of electron, $S_e = 1/2 S_{H_2(g)} = 65.29 J K^{-1} mol^{-1}$, is accounted for [31]. Substituting Eqs. (10a)–(10c) into Eq. (9), the entropy term reads:

$$Q_s = -T \frac{\Delta S_2}{4F} (1-\gamma) I \quad (11)$$

When the efficiency of the oxygen cycle is 100% ($\gamma = 1$), this term is equal to zero.

(b) Ohmic heat term

$$Q_{Ohm} = I^2 R_{el} = I(\varphi^+_{el} - \varphi^-_{el}) \quad (12)$$

φ_{el}^{+} and φ_{el}^{-} are the electrolyte potentials at the electrolyte/positive plate and electrolyte/negative plate interfaces, respectively. This term is always positive and represents the heat generated by the electrolyte resistance. This term may become important at high currents or low saturation levels, when the resistance of inter-electrode volume may increase due to formation of great number of gas bubbles inside the cell.

(c) Overpotential term:

$$Q_\eta = \sum_i I_i \eta_i \tag{13}$$

It represents the heating due to the electrochemical reactions resistances. η_i are the overpotentials of the reactions. This term, too, is always positive and is often called "Joule heating due to electrode resistance". The overpotentials of the different reactions at the positive and negative electrodes are expressed as:

$$\eta_i^{+} = \varphi^{+} - \varphi_{el}^{+} - \varphi_i^0, \qquad \eta_i^{-} = \varphi^{-} - \varphi_{el}^{-} - \varphi_i^0 \tag{14}$$

where φ_i^0 are the equilibrium potentials of different electrode reactions and φ^+ and φ^- are the positive and negative plate potentials. Substituting the expressions for the reaction currents, Eq. (10a)–(10c), and for the overpotentials of the reactions, Eq. (14), into Eq. (13) the expression for the overpotential heat source term reads:

$$Q_\eta = I[U - (\varphi_{el}^{+} - \varphi_{el}^{-}) - (1-\gamma)(\varphi_{O_2}^0 - \varphi_{H_2}^0)],$$

$$\varphi_{O_2}^0 = 1.229\,\text{V}, \quad \varphi_{H_2}^0 = 0\,\text{V} \tag{15}$$

where $\varphi_{O_2}^0$ and $\varphi_{H_2}^0$ are the standard electrode potentials of reactions (2) and (3) against SHE and $U = (\varphi^+ - \varphi^-)$ is the cell voltage.

Substituting Eqs. (11), (12) and (15) into Eq. (8) we obtain the expression for the total heat generation rate:

$$Q_{cell} = I\left[U - (1-\gamma)\left(T\frac{\Delta S_2}{4F} + \varphi_{O_2}^0 - \varphi_{H_2}^0\right)\right] \tag{16}$$

Thermal balance of the cell: For a single cell with immobilized electrolyte and small thickness it can be assumed that the temperature distribution inside the cell is uniform. Then the differential equation that describes the temperature changes can be reduced to the lumped-parameter model of energy balance, e.g. [32].

$$\frac{d}{dt}(C_p T) + hA_{cell}(T - T_a) = Q_{cell} \tag{17}$$

where C_p is the cell thermal capacity, h is the overall heat transfer coefficient, A_{cell} is the surface area of the cell and T_a is the ambient temperature. The second term on the left-hand side represents the effect of heat transfer from the battery to the ambient air.

In this work we will consider the thermal behavior of a VRLA cell at steady state conditions, hence the time derivative term in Eq. (17) is zero and the thermal balance is reduced to

$$hA_{cell}(T - T_a) = Q_{cell} \tag{18}$$

Substituting the expression for the heat generation rate Eq. (16) into Eq. (18) we arrive to the following expression for the temperature vs. current dependence:

$$T - T_a = \frac{I}{hA_{cell}}\left[U - (1-\gamma)\left(T\frac{\Delta S_2}{4F} + \varphi_{O_2}^0 - \varphi_{H_2}^0\right)\right] \tag{19}$$

Eq. (19) shows that when the efficiency of the oxygen cycle is 100%, the energy that is supplied to the system is converted into heat and the increase of the cell temperature depends only on the introduced power and the heat transfer coefficient. At lower efficiencies, part of the energy is removed with the gases leaving the cell.

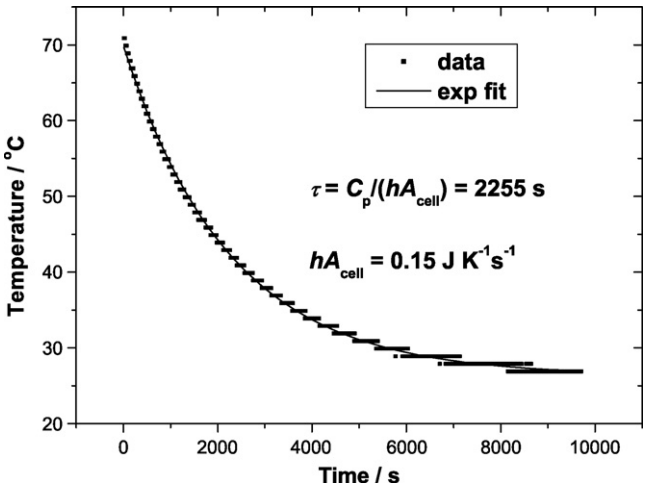

Fig. 1. Cool-down curve. The characteristic time is extracted from an exponential fit and the heat transfer coefficient is calculated: $hA_{cell} = 0.15\,\text{J K}^{-1}\,\text{s}^{-1}$; $h = 5.7\,\text{J K}^{-1}\,\text{s}^{-1}\,\text{m}^{-2}$.

3. Experimental

All experiments were performed with 2 V/4 Ah test cells, comprising 2 mm thick plates (two positive and three negative) separated by 3 mm thick AGM separators. The dimensions of the plates and separator were 5.7 cm × 6 cm, and the dimensions of the cells were 6.5 cm × 3.3 cm × 8.7 cm. Separator sheets were not placed between the box walls and the outermost negative plates. The acid concentration was 1.28 sp.gr. (5 M). All experiments were performed at 90% electrolyte saturation, at which level the cell operates in recombination regime. As the saturation level was sufficiently high and operation of the closed oxygen cycle in the cells was kept stable, it was hardly probable that dry-out of the outer negative plates would occur. Cell current, voltage and temperature, as well as positive and negative plate potentials, were monitored during the experiments. The gas leaving the cells was also measured.

3.1. Cell heat capacity and heat transfer coefficient

The heat capacity of the cell was measured with the help of a self-made calorimeter and the reported value is $C_p = 346.7 \pm 11.5\,\text{J K}^{-1}$.

In order to evaluate the temperature changes it was necessary to consider the effect of heat transfer from the cell to the surroundings. Hence, the overall heat transfer coefficient, h, had to be measured. We measured h for our cell system directly by heating the cell up to 70 °C and then cooling it by natural convection to ambient temperature. From the cool-down curve (Fig. 1) and the value of the heat capacity we obtained the heat transfer coefficient value: $hA_{cell} = 0.15\,\text{W K}^{-1}$; $h = 5.7\,\text{W K}^{-1}\,\text{m}^{-2}$ (the outer area of our test cell was 263.16 cm^2).

The measured heat transfer parameter is within the range reported in the literature for free air convection. It is assumed to be constant throughout the experiments. The temperature dependence on h is neglected because the temperature difference does not exceed 40–50 °C.

3.2. Current/temperature dependence

To measure the characteristic equilibrium T vs. I curves of VRLA cells during stable closed oxygen cycle operation the following experiment was performed. First, the cell was fully charged at galvanostatic regime $I = 0.2$ A and its capacity was checked. Then, the charged cell was put on polarization mode comprising step-wise current changes. Each polarization step continued until constant values of the monitored parameters were achieved. The gassing rate, V_{out}, was also monitored during the experiment. For the sake of brevity, this method will be referred to as *current pyramid* or *galvanostatic pyramid* further in the paper. The maximum applied current was $2\text{ A} = 0.5C_{10}$.

3.2.1. Effect of ambient temperature, T_a

Fig. 2 shows the changes in U, T, φ^+, φ^- and gassing rate as a function of polarization time during galvanostatic pyramidal polarization from $I = 2$ A to $I = 0.2$ A and backwards at 19 °C ambient temperature. Each current change leads to changes in all monitored parameters, which tend to reach stationary values. The transition (non-stationary) period for all monitored parameters lasted up to 3 h.

The experimental data evidence that there is a slight hysteresis in the cell voltage during the downward and upward current steps. But, in general, the cell voltage stays almost constant for currents higher than 0.4 A. The average cell voltage during the experiment is $U = 2.453$ V (Fig. 2a). The changes in cell temperature follow the changes in current: the temperature increases with increase of I and vice verse. The downward and upward steps show that the increase of the cell temperature toward the ambient temperature depends only on I (Fig. 2a).

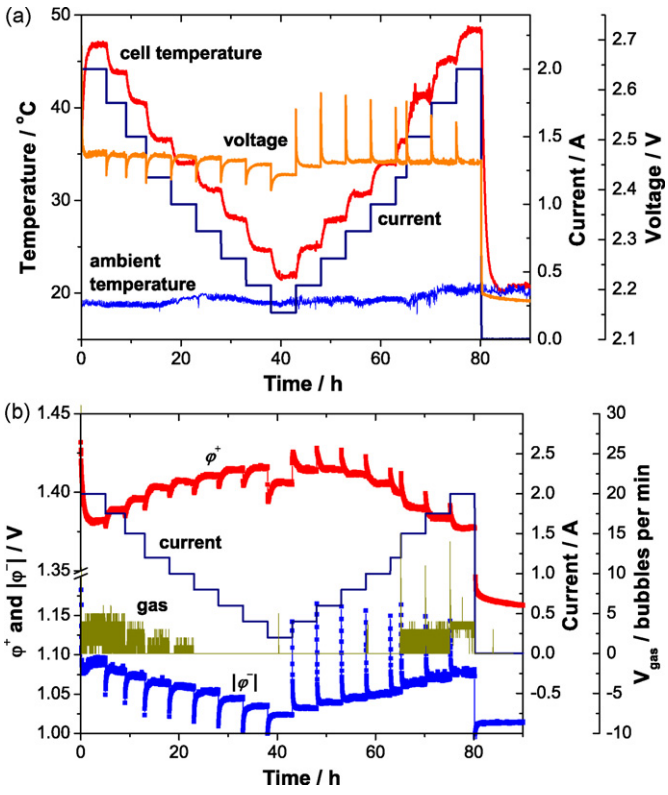

Fig. 2. Galvanostatic pyramidal polarization experiment at $T_a = 19$ °C: (a) cell current, voltage, and temperature; (b) positive and negative plate potentials and gassing rate.

The values of the positive and negative plate potentials measured against Ag/Ag_2SO_4 reference electrode are plotted in Fig. 2b. The positive plate potential depends on both I and T. As the experiment is carried out with fully charged cell, φ^+ is determined only by the kinetics of the OER. On the one hand, at constant temperature, the current increase leads to increase of φ^+. On the other hand, at constant current, φ^+ decreases with increase of T. The competition between these two effects governs the value of φ^+ during step-wise current polarization (Fig. 2b). The value of φ^+ can be determined from the Tafel dependence for OER knowing the kinetic parameters (i.e. activation energy, exchange current and transfer coefficient). In the following subsection we will determine the kinetics of OER.

The polarization of the negative plate increases with I (Fig. 2b). Hence, the overpotential of the hydrogen evolution reaction increases and H_2 may form, which may lead to gassing. The gassing rate of the cell is also plotted in Fig. 2b. It can be seen from the figure that, when the absolute value of the negative plate potential goes above 1.05 V ($|\varphi^-| > 1.05$ V), the cell starts gassing. Hence, for all currents higher than 1A the efficiency of the oxygen cycle is lower than 100%.

Fig. 3 presents the dependences of the equilibrium values of cell temperature as a function of cell current. The data lie on a straight line for all steps for which the cell is in 100% recombination regime (no gassing).

The same stepwise experiment was performed at $T_a = 30$ °C and $T_a = 45$ °C. In order to prevent gassing, the maximum current was chosen so as not to exceed 1 A. The stationary values of T vs. polarization current I are also plotted in Fig. 3. The linear dependence holds for all three experiments:

$$T = T_0 + bI \tag{20}$$

where T_0 is the temperature of the cell at $I = 0$. For these experiments it corresponds to the ambient temperature, $T_0 = T_a$, and b is the slope of the curve. The slopes of the three straight lines are almost the same: $b = 15.2\text{ K A}^{-1}$, 16.1 K A^{-1} and 15.3 K A^{-1} at 19 °C, 30 °C and 45 °C, respectively. The very close values of b for the three experiments indicate that the mechanism of heat generation within the cell does not change and the temperature rise is a direct result of the current increase.

3.2.2. Effect of heat transfer to the surroundings

The experimental cell was put in a thermally isolated box to reduce heat dissipation to the ambient air and the same

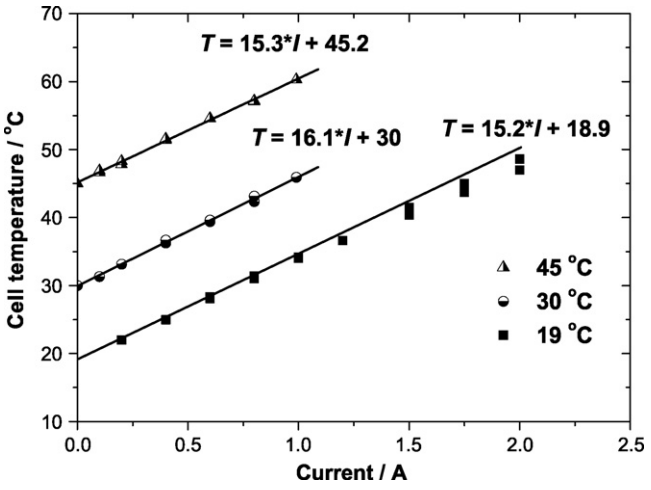

Fig. 3. Dependence of cell temperature on applied current at quasi-steady state conditions in case of free air convection.

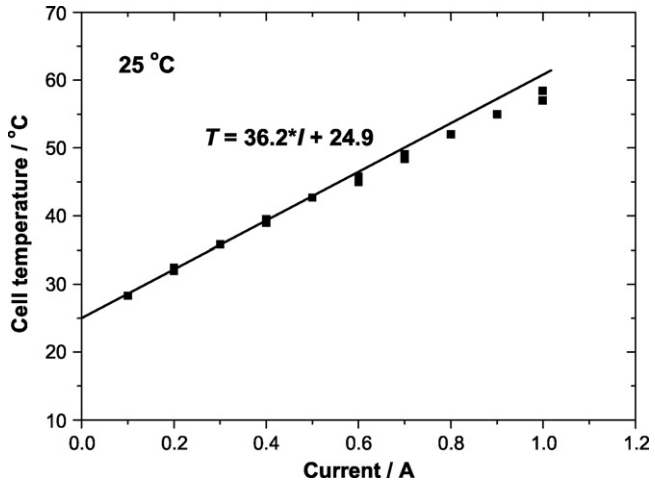

Fig. 4. Dependence of cell temperature on applied current at quasi-steady state conditions: experiment in thermo-box, $T_a = 25\,^{\circ}C$.

galvanostatic pyramidal polarization experiment was performed. The ambient temperature was 25 °C and the maximum applied current was 1 A. The heat transfer coefficient of this wrapped cell was experimentally measured and the obtained value was: $hA_{cell} = 0.061\,W\,K^{-1}$. The stationary temperature/current curve is plotted in Fig. 4 and the variations of the monitored parameters, in Fig. 5. It is evident from the experimental data that the linear temperature/current dependence holds good for non-gassing currents, but the slope has increased more than twice, $b = 36.2\,K\,A^{-1}$, due to restricted heat transfer to the ambient air. All monitored parameters exhibit the same behavior as for the free air convection case (previous subsection).

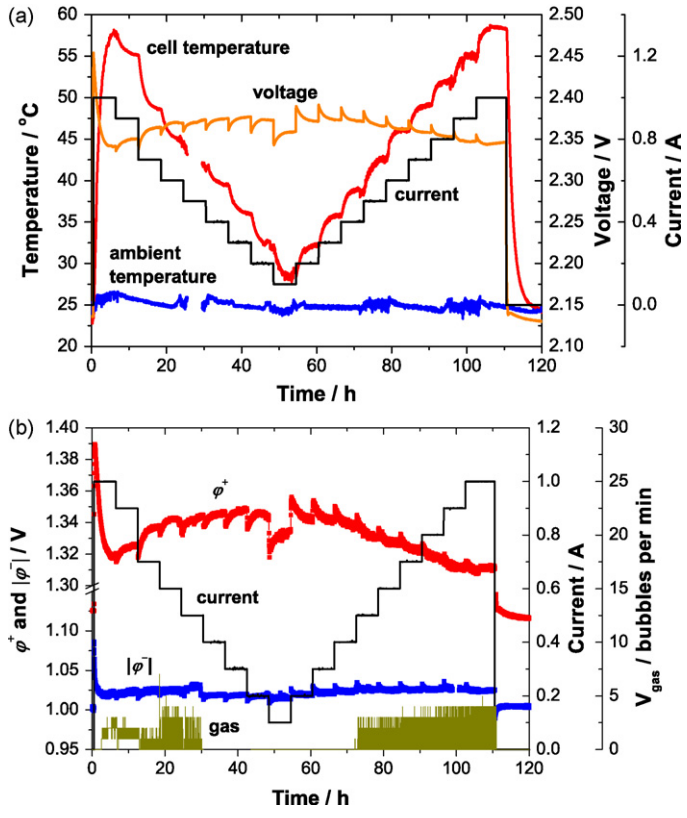

Fig. 5. Galvanostatic pyramidal polarization experiment of the cell in thermo-box at $T_a = 25\,^{\circ}C$: (a) cell current, voltage, and temperature; (b) positive and negative plate potentials and gassing rate.

3.2.3. Thermal characteristics of the cell, b

If we look at the thermal balance, Eq. (19), we can see that the coefficient b is equal to

$$b = \frac{1}{hA_{cell}}\left[U - (1-\gamma)\left(T\frac{\Delta S_2}{4F} + \varphi^0_{O_2} - \varphi^0_{H_2}\right)\right] \quad (21)$$

b is inversely proportional to the heat transfer coefficient. Obviously, if the heat exchange between the cell and the surrounding air is impaired (h is lower), the value of b will increase. This is demonstrated with the experiment in the thermo-box (Fig. 4).

During a single experiment, the heat transfer coefficient h is constant. Hence, the linear T/I dependence is obtained because the group in the brackets is constant. The entropy term in the brackets depends on temperature, but for the temperature interval of the experiment $T \in (20–60\,^{\circ}C)$, it can be considered as constant: it varies between 0.25 V and 0.28 V. In general the cell voltage depends on charging current. For our experiments (see Figs. 2a and 5a), the voltage changes with current within a range of 50 mV and 30 mV, for free air convection and thermo-box experiments, respectively. For the two systems, hA_{cell} is $0.15\,W\,K^{-1}$ and $0.061\,W\,K^{-1}$, respectively. Hence, a cell voltage change of 50 mV will lead to a change of 0.35 °C in cell temperature in the former case and 0.8 °C in the latter. This is within the range of the experimental error for temperature measurements. Hence, the temperature response of our test cell is insensitive to changes in cell voltage within 50 mV (even 100 mV) for these high polarizations.

At 100% efficiency of the oxygen cycle, $\gamma = 1$ and the slope b is: $b = U/(hA_{cell})$. Then, using the average cell voltage values and the measured hA_{cell} values for the two types of experiments (free air convection and thermo-box), the calculated slopes are: $2.453/0.15 = 16.3\,K\,A^{-1}$ and $2.36/0.061 = 38.7\,K\,A^{-1}$, respectively. These values are very close to the experimentally obtained slopes (Figs. 3 and 4).

When the cell is gassing, $\gamma \neq 1$, the second term in the brackets (Eq. (21)) becomes operative. Hence, at high currents, when U remains constant and the cell is gassing (see Fig. 2), the cell temperature is lower than predicted from the linear dependence (see the experimental data at $T_a = 19\,^{\circ}C$ and high currents in Fig. 3).

The presented experimental results show that, when the battery operates at recombination regime, the linear temperature–current dependence holds for all ambient temperatures and heat transfer coefficients. Hence, this slope is a characteristic parameter of the battery and it would be more convenient to present it in dimensionless form:

$$\tilde{b} = b\frac{hA_{cell}}{U_{nom}} \quad (22)$$

where U_{nom} is the nominal voltage of the battery. For the two studied cases (free air convection and thermo-box), the value of $\tilde{b}$ is ≈1.17. This value should be approximately the same for all VRLABs. Hence, $\tilde{b}$ can be used for fast and simple estimation of the thermal response of the battery. One only needs to know the nominal voltage and hA_{cell} of the battery. hA_{cell} is easily measured from the cool-down curve as shown above (see Fig. 1). For example, for a 12 V battery with $hA_{cell} = 1.5\ W\,K^{-1}$ the slope will be $b = 1.17 \times 12/1.5 = 9.36\,K\,A^{-1}$, i.e. a current change of $I = 1$ A will lead to a temperature increase of 9.36 °C.

The experimental data show that the highest increase in cell temperature is observed when the cell is not gassing and the current is the highest at a certain cell voltage U, i.e. the negative plate is com-

pletely depolarized (φ^- is close to its open circuit value $\varphi^- = -1$ V *vs.* Ag/Ag_2SO_4). At these conditions, the cell current is determined only by the kinetics of the OER at the positive plate. The positive plate overpotential will be approximately $\varphi^+ = U - 1$. Hence, knowing the value of the parameter b for a given cell and the kinetics of the OER reaction we can evaluate the cell voltage as a function of ambient temperature, which yields a certain cell temperature. To discuss this, first we will determine the kinetic parameters of the OER in VRLAB.

3.3. Kinetics of the oxygen evolution reaction in recombining VRLA cells

There are numerous studies on the kinetics of the OER on model lead dioxide electrodes in sulfuric acid solution [33–35 and refs. cited therein]. The main question is whether the kinetic parameters of OER are the same when the reaction proceeds on a model electrode in excess electrolyte and on a porous electrode within a cell stack. As oxygen evolution is a gas reaction, its parameters may be affected by the entrapment of formed gas bubbles in the pores of the positive plate and separator when the reaction proceeds in a VRLA cell, which reduces the active surface and contributes to an uncompensated resistance of the pores. For example, the Tafel slopes of OER for plates reported in the literature vary from 75 mV to 110 mV per decade [36–38]. Hence, our aim is to study the kinetics of the OER that proceeds at the positive plate of the test VRLA cell.

Normally, only the OER is expected to proceed at the positive plate:

$$2H_2O \rightarrow O_2 + 4H^+ + 4e^-$$

The corrosion reaction also proceeds therein, but its exchange current is very small, hence, its contribution to the total current compared to the current of OER is considered negligible.

At high overpotentials the reaction current I_{O_2} obeys Tafel relation:

$$I_{O_2} = I = I_0 \exp\left(\frac{\alpha_{a,O_2} F}{RT}\eta\right), \tag{23}$$

where I_0 is the exchange current of the OER at the positive plate, α_{a,O_2} is the charge transfer coefficient, $R = 8.31$ J mol^{-1} K^{-1} is the gas constant and $F = 96487$ C mol^{-1} is Faraday's constant. Eq. (23) can be rewritten in the form:

$$\eta = \varphi^+ - \varphi^0_{O_2} = \frac{RT}{\alpha_{a,O_2} F}(\ln I - \ln I_0), \tag{24}$$

The exchange current depends on temperature. In the simplest form this dependence can be presented as:

$$I_0 = K \exp\left(-\frac{\Delta E^\#}{RT}\right) \tag{25}$$

where K is a coefficient which does not depend on temperature and is a characteristic of the system, and $\Delta E^\#$ is the activation energy of the process.

There are three free parameters in the current/overpotential equation: α_{a,O_2}, K, and $\Delta E^\#$. To evaluate these parameters the test cell was put in a thermo-stated water bath and the I–V characteristics of the fully charged cell were measured at 15 °C, 20 °C, 25 °C, 30 °C and 40 °C. The obtained experimental data are plotted in Fig. 6 (φ^+ is measured vs. Ag/Ag_2SO_4 reference electrode). It can be seen from the figure that, for cell currents lower than 0.1 A, even though the overpotential for OER is high, the current/potential curves start to deviate from Tafel plots. Table 2 summarizes the charge transfer coefficients at different temperatures evaluated from the Tafel

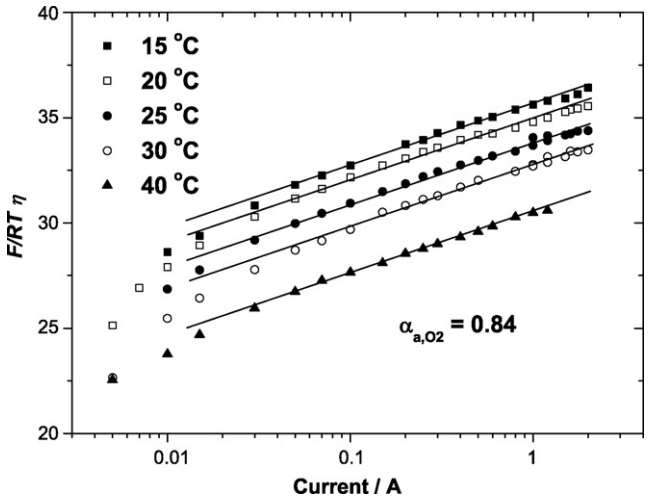

Fig. 6. Current/overpotential curves at different temperatures for the OER during overcharge of VRLA cell.

slope at high overpotentials. There is no indicative dependence of α_{a,O_2} on temperature and it can be assumed that α_{a,O_2} is constant. The obtained average value of α_{a,O_2} is 0.84.

The energy of activation and the constant K can be estimated from the Arrhenius plot. $\ln(I_0)$ vs. T^{-1}. $\ln(I_0)$ is the extrapolated Tafel plot at $\varphi^+ = \varphi^0_{O_2}$.

The standard potential of the oxygen reaction changes with temperature, which has to be accounted for when the value of $\ln(I_0)$ is extracted from the current/potential curves. Our reference electrode is Ag/Ag_2SO_4, whose standard potential against SHE also changes with temperature. The simplest way to account for this dependence is [39]:

$$\varphi^0_i = \varphi^0_i(25\,^\circ\mathrm{C}) + (T - 298)\left(\frac{d\varphi^0_i}{dT}\right) \tag{26a}$$

$$\left(\frac{d\varphi^0_i}{dT}\right) = -\frac{1}{nF}\Delta S. \tag{26b}$$

The values of φ^0_i and $(d\varphi^0_i/dT)$ for O_2/H_2O and Ag/Ag_2SO_4 electrodes are also given in Table 1. The temperature dependence of the standard potential of OER against Ag/Ag_2SO_4 electrode is then

$$\varphi^0_{O_2} = 0.575 + 0.339 \times 10^{-3}(T - 298). \tag{26a}$$

The Arrhenius plot for the exchange current density of oxygen evolution, $\ln(I_0)$ vs. T^{-1}, is presented in Fig. 7. Full squares give the experimental values from the water bath experiment. Other data points in the graph are from the pyramidal polarization experiments in air. For the latter experiments, the $\ln(I_0)$ values are calculated using the experimental values of φ^+, T and I for the current steps at which φ^+ reaches equilibrium, and the measured transfer coefficient $\alpha_{a,O_2} = 0.84$. As expected, all data lie on a uniform straight line. The values of

Table 2
Parameters of the Tafel plot of the oxygen evolution reaction at the positive plate of VRLAB.

T (°C)	α_{a,O_2}	Tafel slope: $RT/\alpha_{a,O_2}F$ (mV per decade)	$\ln(I_0)$ (A)
15	0.853	67	−30.36
20	0.840	69	−29.30
25	0.837	70.5	−28.24
30	0.831	72	−27.18
40	0.825	75	−25.12

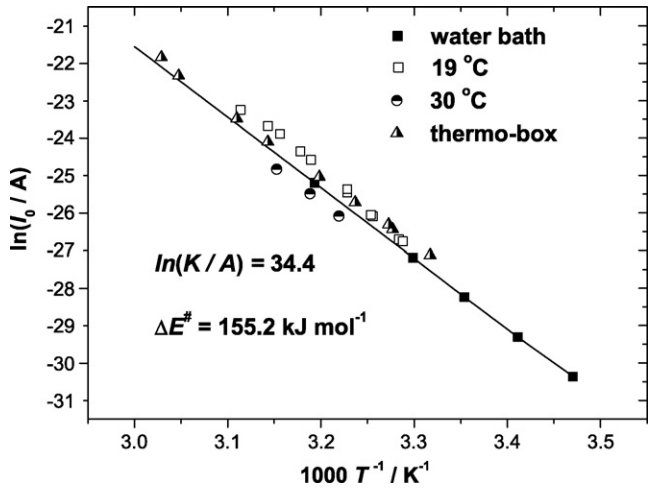

Fig. 7. Arrhenius plot for the OER.

the other two parameters are then extracted from this straight line: $\ln(K,\ \mathrm{A}) = 34.4$ and $E^{\#} = 155.2\ \mathrm{kJ\,mol^{-1}}$. (The small deviations of the experimental points for current polarization from the straight line for the water bath experiment can be ascribed to slightly different active areas of the electrodes in different cells).

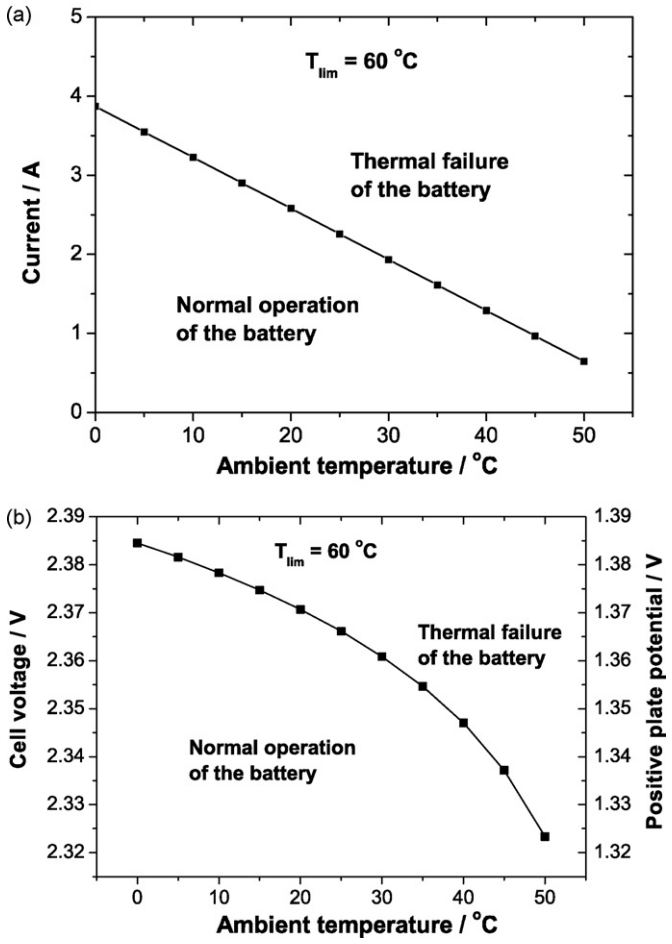

Fig. 8. Critical cell current and voltage as a function of T_a at $T_{lim} = 60\,^{\circ}\mathrm{C}$: (a) current vs. T_a; (b) positive plate potential and voltage vs. T_a.

The effective Tafel slope obtained here is between 67 mV and 75 mV per decade for the temperature range 15–40 °C.

4. Critical conditions for thermal failure of the battery

It is well known that high temperatures are harmful for VRLAB operation because of enhanced corrosion and water evaporation rates. Degradation of the expander of the negative plate starts above a threshold temperature of about 60 °C. Hence, we will assume that $T_{lim} = 60\,^{\circ}\mathrm{C}$ is the limiting temperature for normal battery operation. From the linear current temperature dependence (Eq. (20)) and the value of the parameter b we can calculate the limiting current at which the temperature of the cell reaches 60 °C as a function of ambient temperature. The values obtained for our test cell are plotted in Fig. 8. For a given T_a, the cell will operate normally at all currents below the line in Fig. 8a, whereas at currents above the line, thermal failure of the battery will occur. At float regime, the potential of the positive plates of VRLAB is determined by the kinetics of OER, as was discussed above. Hence, for our test cell we can calculate the limiting positive plate potential at which the cell temperature is 60 °C, as a function of T_a, from the limiting current and the kinetic parameters of the OER reaction. This dependence is plotted in Fig. 8b. As the worst case for heating of the cell is observed when the negative plate potential is close to the equilibrium one (open circuit), $\varphi^{+} = -1$ V vs. Ag/Ag_2SO_4, then the limiting safe polarization voltage is $U = \varphi^{+} + 1$ V. Critical cell voltages are also plotted in Fig. 8b. At all voltages bellow the curve the cell will operate normally, while at voltages above the curve it may suffer thermal failure.

5. Conclusions

The present work shows that, at electrolyte saturations of around 90%, the thermal behavior of the VRLA cell is determined only by the charging current and the heat transfer to the surroundings. For small temperature changes, in the range of 50–70 °C, which is the case with VRLA batteries, the overall heat transfer coefficient is constant. The experiments show that, for recombination cells, the cell temperature is linearly proportional to the charging current. When the cell is gassing, part of the heat is dissipated with the gases that leave the cell and the cell temperature is lower than predicted from the linear temperature/current dependence.

The dimensionless slope $\tilde{b}$ can be used for simple and fast estimation of the thermal response of a VRLA battery to cell current changes.

On overcharge, the value of the positive plate potential is determined by the kinetics of the oxygen evolution reaction. In the present work, the kinetic parameters of OER proceeding at the positive plate of VRLA cell are determined. The current/potential dependence of the OER obeys Tafel relation. The experimental results obtained indicate that the charge transfer coefficient of the OER proceeding at the positive plate of hermetically sealed lead-acid cell is constant and its value is higher than that measured for PbO_2 electrodes in H_2SO_4 solution (the Tafel slope is smaller compared to flooded PbO_2 electrodes).

The most critical conditions for self-heating of the VRLA cell is when the negative plate is least polarized, i.e. the value of φ^{-} is close to its equilibrium (open circuit) value. Otherwise, the overpotential of the hydrogen evolution reaction becomes high enough and the cell starts gassing. Using the linear T/I dependence, the φ^{+} value calculated for given I and T, and the open circuit value of φ^{-}, it is possible to predict the limiting charging float voltage for safe operation of the battery.

Acknowledgement

The authors are grateful to Dr. H. Catherino for the constructive discussion and acknowledge with thanks the financial support provided by the European Research Office of the U.S. Army for carrying out this research (contract number N62558-06-P-0070).

References

[1] H.F. Gibbard, J. Electrochem. Soc. 125 (1978) 353.
[2] W.G. Eicke Jr., J. Electrochem. Soc. 109 (1962) 364.
[3] D. Berndt ad, E. Meissner, Proceedings of the 12th Telecommunications Energy Conference (INTELEC 90), Orlando, FL, USA, 1990, p. 148.
[4] S.S. Misra, T.N. Noveske, A.W. Williamson, Proceedings of the 14th Telecommunications Energy Conference (INTELEC 92), Washington, DC, USA, 1992, p. 186.
[5] S.D. Gerner, G.H. Brilmyer, D.H. Bornemann, Proceedings of the 12th Telecommunications Energy Conference (INTELEC 90), Orlando, FL, USA, 1990,p. 161.
[6] S.S. Misra, A.W. Williamson, Proceedings of the 20th Telecommunications Energy Conference (INTELEC 98), San Francisco, CA, USA, 1998,p. 536.
[7] R.K. Jaworski, J.M. Hawkins, Proceedings of the 18th Telecommunications Energy Conference (INTELEC 96), Boston, MA, USA, 1996, p. 45.
[8] M. Hoff, K. Steeves, Proceedings of Battcon 2005 Conference, Miami Beach, FL, USA, 2005, pp. 12–21.
[9] P. Haering, H. Giess, J. Power Sources 95 (2001) 153.
[10] F.A. Fleming, B. Philip Shumard, Dickinson, J. Power Sources 78 (1999) 291.
[11] H. Catherino, J. Power Sources 158 (2006) 977.
[12] A. Pesaran, M. Keyser, Proceedings of the 16th Annual Battery Conference: Advances and Applications, Long Beach, CA, 2001, p. 219.
[13] A. Pesaran, A. Vlahinos, S.D. Burch, Thermal performance of EV and HEV battery modules and packs, in: Proceedings of the 14th Electric Vehicles Symposium, Orlando, FL, December 12–17, 1997.
[14] A. Pesaran, D.J. Russel, J.W. Crawford, R. Rehn, E.A. Lewis, A unique calorimetric-cycler for evaluating high-power battery modules, in: Proceedings of the Long Beach Battery Conference, January, 1998.
[15] B. Culpin, J. Power Sources 133 (2004) 79.
[16] B. Culpin, K. Peters, J. Power Sources 144 (2005) 313.
[17] J. Hu, Y. Guo, X. Zhou, J. Appl. Electrochem. 36 (2006) 1083.
[18] D. Pavlov, J. Power Sources 64 (1997) 131.
[19] A. Kirchev, D. Pavlov, B. Monahov, J. Power Sources 113 (2003) 245.
[20] D. Pavlov, A. Kirchev, B. Monahov, J. Power Sources 144 (2005) 521.
[21] D. Pavlov, B. Monahov, A. Kirchev, D. Valkovska, J. Power Sources 158 (2006) 689.
[22] D. Pavlov, J. Power Sources 158 (2006) 964.
[23] A.I. Harrison, Proceedings of the 14th Telecommunications Energy Conference (INTELEC 92), Washington, DC, USA, 1992, p. 28.
[24] S. Torigoe, K. Matsumoto, K. Maki, T. Tanaka, T. Babasaki, Proceedings of the 16th Telecommunications Energy Conference (INTELEC 94), Vancouver, BC, Canada, 1994, p. 54.
[25] H. Huang, T. Nguyen, J. Electrochem. Soc. 144 (1997) 2420.
[26] D. Berndt, U. Teutsch, J. Electrochem. Soc. 143 (1996) 790.
[27] J.J. Lander, J. Electrochem. Soc. 98 (1951) 213.
[28] A. Arlanch, G. Clerici, M. Maja, J. Power Sources 8 (1981) 581.
[29] K.R. Bullock, W.H. Tiedemann, J. Electrochem. Soc. 127 (1980) 2112.
[30] D.R. Lide (Ed.), Handbook of Chemistry and Physics, 79th ed., CRC Press, 1997.
[31] M.J. Lampinen, M. Fomino, J. Electrochem. Soc. 140 (1993) 3537.
[32] C.Y. Wang, V. Srinivasan, J. Power Sources 110 (2002) 364.
[33] M. Pathy, H. Udupa, Electrochim. Acta 10 (1965) 1185.
[34] M. Dimitrov, J. Power Sources 31 (1990) 121.
[35] D. Pavlov, B. Monahov, J. Electrochem. Soc. 145 (1998) 70.
[36] D. Bernardi, R. Ying, P. Watson, J. Electrochem. Soc. 151 (2004) A85.
[37] F.J. Vaccaro, E. Landwehrle, Proceedings of the 13th Telecommunications Energy Conference (INTELEC 91), Kyoto, Japan, 1991, p. 20.
[38] F.J. Vaccaro, J. Rhoades, B. Le, Proceedings of the 19th Telecommunications Energy Conference (INTELEC 97), Melbourne, Vic., Australia, 1997, p. 230.
[39] H. Bode, Lead-Acid Batteries, John Wiley & Sons, Inc., New York, 1977, p. 94.